Catalysis Today 459 (2025) 115425

Contents lists available at ScienceDirect

Catalysis Today

journal homepage: www.elsevier.com/locate/cattod

Influence of Mg loadings in copper-based catalysts for CO_2 hydrogenation to methanol

Maria Dore [a,b], Cristina Peinado [a], Sergio Rojas [a], Jose M. Campos-Martin [a], Dalia Liuzzi [a,*], Silvia Morales-delaRosa [a,*]

[a] Sustainable Energy and Chemistry Group (EQS), Instituto de Catálisis y Petroleoquímica, CSIC, C/ Marie Curie 2, Cantoblanco, Madrid 28049, Spain
[b] Escuela de Doctorado, UAM, Madrid 28049, Spain

ARTICLE INFO

Keywords:
CO_2 hydrogenation
Copper-based catalysts
Magnesium loadings
Methanol
CCU

ABSTRACT

The conversion of carbon dioxide (CO_2) to methanol offers a sustainable route to mitigate greenhouse gas emissions while producing a key chemical feedstock. In this study, we investigate the effect of magnesium (Mg) loadings on the performance of copper-based catalysts for CO_2 hydrogenation to methanol. Catalysts based on $Cu/ZnO/Al_2O_3$ (CZA) were synthesized via co-precipitation and modified with varying amounts of Mg to yield Mg-promoted samples (CZAM). Comprehensive characterization using X-ray diffraction, N_2 adsorption–desorption isotherms, H_2 temperature-programmed reduction, and N_2O chemisorption revealed that moderate Mg incorporation decreases Cu crystallite size and enhances the BET surface area, thereby improving copper dispersion. Catalytic tests conducted at 240 °C and 50 bar with varying Gas Hourly Space Velocities (GHSV) showed that an intermediate Mg loading (approximately 0.8 wt%) yields optimal performance, achieving a CO_2 conversion of 23.3 % and methanol selectivity of 55 %, comparable to that of a commercial catalyst. Excessive Mg content, however, adversely affects dispersion and selectivity despite higher intrinsic site activity. Stability tests over 120 h confirm sustained catalytic performance under reaction conditions. These results demonstrate that careful control of Mg loading and GHSV is critical to optimize catalyst structure and activity, offering insights for developing catalysts for sustainable methanol production from CO_2.

1. Introduction

The reduction of all contributing factors to global warming is now an essential measure and one of the most important challenges of our century [1]. The latest agreement signed by Europe in 2021, "Fit for 55" set the goal of reducing emissions by 55 % by 2030 and achieving carbon neutrality by 2050 [2]. Among the greenhouse gases emitted by human activities, carbon dioxide (CO_2) is certainly the most abundant, and although it is a relatively weak greenhouse gas, it is considered the main driver of global warming [1,3]. The issue is not CO_2 itself, which is a naturally occurring and non-toxic gas, but rather its excessive concentration has risen extremely, from roughly 280 ppm in pre-industrial times to over 420 ppm today. In this context, proposed solutions range from eliminating the causes of anthropogenic CO_2 emissions to reducing the concentration of CO_2 already present in the atmosphere [4]. In this latter category belongs research on CCS and CCU technologies [5], which stand for Carbon Capture and Storage and Carbon Capture and Utilization, respectively. In CCS technologies, CO_2 is simply stored in systems where it is no longer released as free gas [6], while in CCU technologies, the captured CO_2 is converted into more useful products [7,8]. The advantage of CCU is that it aims to recycle CO_2, which is highly abundant, using it as a C_1 building block to produce value-added fuels, chemicals, and materials [9].

The catalytic conversion of CO_2 to methanol has attracted significant attention because it produces a crucial industrial intermediate. Methanol, together with ethylene, propylene, and ammonia, is considered one of the four building blocks of the chemical industry and serves as a key precursor for a wide range of commercial products [10]. Additionally, methanol can be considered an ideal clean liquid fuel for vehicles and a potential fuel additive for reducing hydrocarbon emissions from diesel engines [9,11,12]. Methanol is already used in maritime applications due to its ease of storage as a liquid at ambient temperature and its low emissions of sulfur oxides (SO_X) and particulate matter, aligning with strict environmental regulations [13,14]. Furthermore, pure

* Corresponding authors.
E-mail addresses: dalia.liuzzi@csic.es (D. Liuzzi), smorales@icp.csic.es (S. Morales-delaRosa).

https://doi.org/10.1016/j.cattod.2025.115425
Received 27 February 2025; Received in revised form 30 April 2025; Accepted 12 June 2025
Available online 14 June 2025
0920-5861/© 2025 The Authors. Published by Elsevier B.V. This is an open access article under the CC BY license (http://creativecommons.org/licenses/by/4.0/).

methanol engines have demonstrated the ability to achieve efficiencies close to 43 % and maintain them above 40 % across a wide range of speeds and loads [15].

The various uses of methanol, both as a chemical intermediate and a direct fuel, have led to a significant increase in its production and consumption, rising from 51.7 million tons per year in 2011 to 98 million tons per year in 2020. Of this amount, 69 % is allocated to chemical applications, while 31 % is used as fuel. By 2025, this growth trend is projected to reach nearly 110 million metric tons per year [16].

The conversion of CO_2 to methanol through hydrogen reduction in heterogeneous catalysis is one of the most commonly used methods [9]. The most widely used industrial catalyst is a copper-based system with the formula $Cu/ZnO/Al_2O_3$, known as CZA [17–20]. Commercial CZA catalysts typically consist of 60 wt% Cu, 30 wt% ZnO, and 10 wt% Al_2O_3 [9,20]. In this case, the reactions involved in the interaction between CO_2, the catalyst, and hydrogen are the following:

(1) $CO_2 + 3\ H_2 \leftrightarrow CH_3OH + H_2O$ $\quad \Delta H_{298\ K} = -49.5\ KJ\ mol^{-1}$

(2) $CO + 2\ H_2 \leftrightarrow CH_3OH$ $\quad \Delta H_{298\ K} = -90.4\ KJ\ mol^{-1}$

(3) $CO_2 + H_2 \leftrightarrow CO + H_2O$ $\quad \Delta H_{298\ K} = +41.5\ KJ\ mol^{-1}$

Where (1) and (2) are the methanol formation reactions from CO_2 and CO respectively and both are exothermic; while reaction (3) is the reverse water-gas shift reaction (RWGS) and is endothermic [21].

The extensive use of CZA in industrial methanol synthesis is well established due to CZA high catalytic activity, long lifetime, resistance to poisoning, and relatively low reaction temperature and pressure [9,22]. Additionally, it is cost-effective and easy to synthesize [23]. Nevertheless, improving its properties remains a topic of intense research [22] in which many efforts have focused not only on optimizing the CO_2 reduction parameters [24] but also on implementing the catalyst preparation methods and catalyst composition [9].

The reaction mechanism for methanol synthesis from CO_2 on Cu-based catalysts has been widely studied. DFT studies propose two main pathways, depending on the intermediate involved. The first proceeds via formate generation, while the second involves carboxyl and subsequently formyl species. However, the latter appears kinetically disfavoured on copper catalysts, making the formate pathway the more plausible [25]. In this mechanism, H_2 is adsorbed and dissociated on metallic Cu, while CO_2 adsorbs on ZnO sites. The resulting hydrogen atoms react with CO_2 to form formate ($HCOO^-$) and other intermediates, which are further hydrogenated on Cu sites to yield methanol [26]. Although other C_1 products such as HCOOH and HCHO can form, their low stability leads to further hydrogenation to methanol, which is thermodynamically favoured. More reduced products like CH_4, C_2H_4, and C_2H_5OH are also thermodynamically possible but are rarely observed with Cu-based catalysts [25].

It is broadly recognized that synthesis methods play a crucial role in determining catalyst properties [9,27,28] and in the case of CZA synthesis, co-precipitation is the most extensively used on an industrial scale [29–31]. Also, sol–gel [32] and impregnation [33] methods can be used. Composition is another fundamental parameter as it influences catalyst properties like surface basicity, which is widely accepted and supported by evidence, that is pivotal in the interaction with CO_2. In fact, since CO_2 has acidic properties, the catalyst surface alkalinity influences its adsorption [34]. Also, the strength and number of basic sites affect methanol selectivity [35]. It also was observed that composition variations strongly influence the properties of metallic copper (Cu^0) including crystallite size, surface area, dispersion, as well as catalyst surface area, and acid-base characteristics [36]. Since Cu^0 is considered the active site [37,38], these changes are directly linked to the catalyst's activity. Recent studies, including operando characterizations, have highlighted that the Cu^0-ZnO interface plays a crucial role in enhancing catalytic performance by promoting both CO_2 adsorption and H_2 activation [39]. In this context, ZnO acts not only as a structural stabilizer but also as an electronic promoter, facilitating charge transfer processes at the interface.

Thus, the composition can have a substantial impact on the catalyst performance. In $Cu/ZnO/Al_2O_3$-based catalysts, each component plays a distinct role in determining catalytic performance. Metallic Cu^0 is widely recognized as the active site for CO_2 hydrogenation, while ZnO acts as a structural and electronic promoter, enhancing Cu dispersion and stability. Al_2O_3 serves as a robust support, contributing to surface area and thermal resistance. The incorporation of Mg introduces additional basicity and structural modifications, which can further enhance CO_2 adsorption and copper dispersion, but may also impact selectivity if not properly balanced [36,40].

This is a well-known strategy used to improve catalyst properties; in fact, numerous studies have demonstrated that the incorporation of additives in Cu-based catalysts (e.g. metal oxides, noble metals, etc.) increases the Cu^0 dispersion and modifies acid-base properties and redox properties, enhancing the catalytic performance and stability; thus, acting as promoters [9,17,41,42]. Among these, it has been extensively observed that adding Mg into copper-based catalysts can improve catalytic performances, even in the case of more simple systems like Cu/ZnO [36,43–45], Cu/Al_2O_3 [34,46] or Cu/ZrO_2 [47]. In all these studies, a common positive effect promoted by magnesium was evidenced in the structure (larger surface area and higher dispersion of the Cu active sites), the reactivity (increase in the basicity of the catalyst), and stability [48].

In a DFT study conducted on a Cu-based catalyst promoted by Mg [49], it was shown that the CO_2 absorption energy on a Cu/MgO system was −1.25 eV, which was 0.56 eV stronger than the absorption on a Cu/ZnO system (-0.69 eV), probably due to the basic nature of Mg, as the authors stated. The calculation of the CO_2 absorption energy on the Cu/MgO/ZnO system (-1.04 eV) further supported the idea that the presence of Mg could potentially enhance CO_2 absorption on the copper-based catalyst surface, compared to a simple Cu/ZnO system.

The influence of Mg on specific $Cu/ZnO/Al_2O_3$ composition loadings has also been observed in a few studies. Ledakowicz et al. [50] found that Mg-promoted CZA catalyst increased the methanol activity mainly owing to the enhancement of the BET surface area. Zhang et al. [51] improved the BET surface area and Cu dispersion of the CZA catalysts with Mg, but no significant differences were observed in catalytic activity, and even a slight decrease was noted. A similar unfavorable impact was observed by Beiramar et al. [52], where the addition of Mg did not improve the activity but rather slightly reduced the surface area. Previtali et al. [53] observed that the basic character of Mg slightly increased the surface area, but no data on catalytic activity were reported. Ay et al. [54] observed that the addition of the Mg promoter resulted in a larger surface area and smaller CuO particles, although a detrimental effect was observed on catalyst activity. In a more recent work, Wang et al. [55] obtained a catalyst with smaller Cu particles sizes with higher dispersion, by adding Mg to CZA. This is the only case in which a CO_2/H_2 mixture was used for catalytic activity tests. They achieved 10 % of CO_2 conversion, 80 % of methanol selectivity and displayed high stability for 120 h at 190 °C, 30 bar and 10,000 mL g_{cat}^{-1} h^{-1}. In all these studies, CZA with Mg was prepared using the co-precipitation method.

To the best of our knowledge, for $Cu/ZnO/Al_2O_3$ systems, data on CO_2 conversion in methanol synthesis from CO_2/H_2 mixtures and the effect of different Mg loadings are still lacking. Also, there is a complete absence of data on the influence of Gas Hourly Space Velocity (GHSV) on its catalytic activity.

In this work, we prepared and characterized three different CZA catalysts for methanol synthesis from a CO_2/H_2 mixture with the co-precipitation method, using different loadings of Mg considered in the form of magnesium oxide (MgO) and a range of GHSV for catalytic activity tests. We also studied a commercial copper-based catalyst, characterized with the same techniques and conditions. The MgO loadings selected in this study (0, 2, and 5 wt%) were chosen based on previous literature and our preliminary results, aiming to explore key behavioural regimes: absence of promoter, moderate promotion, and excessive

promotion. Although these values are not equally spaced, this approach allows capturing the main structural and catalytic effects associated with MgO addition without requiring a full parametric study. Similar strategies have been employed in recent works on MgO-promoted Cu-based catalysts, where non-equidistant MgO loadings were selected to optimize catalytic behaviour and surface properties [40,56].

2. Materials and methods

2.1. Synthesis of catalysts

$Cu/ZnO/Al_2O_3$ (CZA) and $Cu/ZnO/Al_2O_3/MgO$ (CZAM) catalysts were synthesized by the co-precipitation method. The amount of Mg added as a promoter was calculated based on the corresponding MgO content, ranging from 0 % to 5 % (wt%), while the molar percentages between metal elements Cu, Zn and Al were kept respectively at 66 %, 27 % and 7 % for all catalysts.

Co-precipitation was realized using metal nitrates as starting materials, under basic conditions and controlled temperature. The solution of the precursors was prepared by dissolving appropriate amounts of Cu $(NO_3)_2{\cdot}3\ H_2O$ (99.5 %, Johnson Matthey-Alfa), $Zn(NO_3)_2{\cdot}6\ H_2O$ (98 %, Sigma Aldrich), $Al(NO_3)_3{\cdot}9\ H_2O$ (>99 %, Fluka) and $Mg(NO_3)_2{\cdot}6\ H_2O$ in 100 mL of deionized water, to give a total 2 M concentration for the metal salts. The basic solution was prepared with Na_2CO_3 (98 %, Alfa-Aesar) in deionized water (1.6 M).

The precursor solution was slowly poured into a 500 mL glass reactor, previously filled with 200 mL of deionized water, at 65 °C under continuous stirring, carefully maintaining the pH with the simultaneous addition of the Na_2CO_3 solution. The catalyst without magnesium was prepared at pH= 8, and all compositions with magnesium were prepared at pH= 7. After co-precipitation, the suspension was kept under stirring, at 70 °C for 1 h and then aged at room temperature for 24 h. Then, it was filtered under vacuum, rinsing several times with deionized water until the pH value of the washing medium was 7. The precipitates were dried at 80 °C overnight and calcined at 320 °C for 2.5 h with a heating rate of 2 °C·min^{-1}. The catalysts obtained were labeled as CZA for the composition without magnesium, CZAM_2 for the composition with 2 % MgO (wt%) and CZAM_5 for the composition with 5 % MgO (wt%).

The characterization and catalytic activity results were compared with a commercial catalyst purchased from Alfa Aesar (ref. 045776).

2.2. Characterization of catalysts

Powder X-ray diffraction (XRD) qualitative analysis was performed to identify all crystallographic phases. XRD patterns of powder samples were collected in a X'Pert Pro PANalytical with a θ–θ configuration, CuKα radiation (λ=1.5406 Å, 45 kV, 40 mA), and equipped with a X'Celerator detector. Measurements were performed over a 2θ range of 4–90, using 0.04° as step size and 20 s of integration time. XRD analysis in reaction chamber (Anton Paar XRK900) was realized by heating up to 300 °C in a reducing atmosphere (H_2/N_2), with a heating rate of 2.5 °C·min^{-1}. The crystallite size of the Cu particles (d_{Cu}) was determined by the Scherrer equation as follows:

$$d_{Cu} = K\lambda/\beta\cos\theta \tag{1}$$

where K = 0.94, assuming a cubic symmetry of the Cu particles, λ is the wavelength of the X-ray source (1.5406 Å), β is the full width at half maximum (FWHM) of the peak at position θ. For the synthesized catalyst, XRD analysis was carried out only on calcined samples.

N_2 adsorption-desorption isotherms were realized in an Asap2020 Micromeritics, previously degassing the samples at 140 °C in a VacPrep 061 LB Micromeritics. Catalyst surface area was determined by BET method, and pore size distribution was derived by the BJH method based on the desorption branch.

Temperature-programmed reduction (H_2-TPR) was performed in a TPD/TPR 2900 from Micromeritics equipped with a thermal conductivity detector (TCD) to study catalyst reducibility. Analysis was carried out by heating up to 700 °C (10 °C·min^{-1}) in a reducing H_2/Ar atmosphere, previously drying the catalyst at 120 °C for 30 min under inert gas flow (He).

In the same apparatus (TPD/TPR 2900 – Micromeritics), N_2O chemisorption was realized in order to quantify the number of active sites on the catalyst surface. As done for the TPR analysis, after being dried at 120 °C for 30 min in an inert atmosphere (He), the catalyst was reduced under H_2/Ar flow by heating from room temperature to 250 °C (2 °C·min^{-1}). After that, the catalyst was cooled up to room temperature in an inert atmosphere (He), and then it was treated with N_2O (2 % in Ar) for 15 min to oxidize the surface Cu atoms. Non-chemisorbed N_2O was purged from the reactor by flowing He during 30 min. Then, a second TPR was carried out, heating up to 250 °C in H_2/Ar flow with a heating ramp of 10 °C·min^{-1}. From the data acquired in this analysis, it was possible to derive Cu dispersion (D_{Cu^0}), the number of Cu^0 exposed active sites (Cu^0_{sites}) and also the superficial area of all Cu^0 sites on the catalyst surface (S_{areaCu^0}), by measuring the hydrogen absorbed in the first reduction (A_i) and hydrogen absorbed in the second reduction (A_{ii}). This is because the first reduction involves the whole catalyst, while the second one affects only surface atoms previously oxidized by N_2O. The amount of hydrogen consumed for the reduction of surface copper was determined by deconvoluting the first peak of the second reduction profile, which, according to the literature [57], corresponds to the reduction of Cu^+ species formed via N_2O chemisorption. The equations used to determine these parameters are the following:

$$D_{Cu^0}(\%) = \frac{2\,(A_{ii})}{A_i} \times 100\% \tag{2}$$

$$Cu^0{}_{sites}\ \left(mol_{Cu}{\bullet}g_{cat}{}^{-1}\right) = \frac{D_{Cu^0} \bullet [Cu]}{AW_{Cu}{\cdot}10000} \tag{3}$$

$$S_{area_{Cu^0}}\ \left(m^2{\bullet}g_{cat}{}^{-1}\right) = Cu^0{}_{sites}A_{Cu^0}N_A \tag{4}$$

Where 2 in (2) equation is the stoichiometric number of the reaction: $Cu_2O + H_2 \rightarrow 2Cu + H_2O$, [Cu] is the wt% of Cu in the catalyst, AW_{Cu} is the atomic weight of Cu, A_{Cu^0} is the surface area of a single Cu atom (6.85 Å^2 [31]) and N_A is the Avogadro constant.

Inductively coupled plasma-mass spectrometry was realized on synthesized and commercial catalysts, using an ICP-MS NexION 300X - Perkin Elmer spectrometer, to determine the elemental composition.

The basicity of the catalysts was evaluated by CO_2 temperature-programmed desorption (CO_2-TPD). Prior to analysis, approximately 50 mg of catalyst was pre-treated under a flow of Helium (50 mL·min^{-1}) at 100 °C for 30 min to remove physisorbed species. Subsequently, the catalyst was reduced under a H_2/Ar mixture up to 250 °C (ramp: 5 °C·min^{-1}) for 30 min to ensure proper activation of the copper sites. After cooling down to 50 °C under Ar (50 mL·min^{-1}), the catalyst was exposed to pure CO_2 flow (25 mL·min^{-1}) for 1 h to allow adsorption.

The physiosorbed CO_2 was removed by purging with He (50 mL·min^{-1}) for another hour at room temperature. The TPD was then carried out by heating the sample up to 800 °C at a rate of 10 °C·min^{-1} under He flow (50 mL·min^{-1}). The desorbed species were monitored using both a thermal conductivity detector (TCD) and a mass spectrometer (MS). The MS was set to track specifically the $m/z = 44$ signal to ensure that the detected desorption peaks corresponded exclusively to CO_2, ruling out interference from other possible species such as H_2O ($m/z = 18$) or CO ($m/z = 28$).

2.3. Catalytic activity tests

Catalytic performance tests were carried out in a stainless steel fixed-bed tubular reactor placed in a furnace and fed by a gas supply unit (three high-pressure cylinders: N_2, H_2, and $CO_2/H_2/N_2$ mixture). In this setup, gas flows coming from the feed unit are controlled before entering

the reactor, the reaction temperatures are monitored by a thermocouple placed in the center of the catalytic bed, and pressure is regulated by an automatic valve at the reactor outlet.

The catalytic bed was prepared to give a total volume of 0.8 cm^3, mixing 200 mg of catalyst with 0.6 cm^3 of silicon carbide (SiC) to dissipate the heat produced in the reaction. The catalyst powder was sieved beforehand to obtain a diameter of 250–300 μm.

Prior to each reaction, the catalyst was reduced for 2.5 h at 250 °C and atmospheric pressure, in a H_2/N_2 (20/80 vol.) flow, with a heating ramp of 2 °C·min^{-1}. Then, catalytic activity tests were carried out at 240 °C, 50 bar, and fed with the gas mixture $CO_2/H_2/N_2$ (vol% composition: 22/68/10 respectively) with N_2 serving as the internal standard. The temperature and pressure were selected based on prior optimization studies and literature data, where Cu-based catalysts exhibit the best balance between CO_2 conversion and methanol selectivity [58,59]. Higher temperatures, although favourable for CO_2 conversion, are known to promote the RWGS reaction, reducing methanol yields. Therefore, this temperature was chosen to ensure a meaningful comparison of catalyst performance under optimized and industrially relevant conditions. The GHSV gradually increased from 2500 h^{-1} to 15, 000 h^{-1}, with steps of 2500 h^{-1}, and then reduced again to 2500 h^{-1} to estimate possible deactivation. Each GHSV value was maintained for 7 h, giving a total time on stream (TOS) of 49 h.

Outlet gas composition was analysed by an online gas chromatograph (Agilent 8890 GC System) equipped with TCD and FID detectors. In order to calibrate the TCD detector, the inlet gas composition was previously analysed before starting reactions. Also, a separate calibration was realized using a CO/N_2 feed to determine the TCD response factor to CO. The FID detector was calibrated with pure standards. From acquired chromatograms data, the CO_2 conversion ($\mathscr{X}_{CO_2}$), methanol selectivity (S_{MeOH}), carbon monoxide selectivity (S_{CO}), methanol productivity (STY_{MeOH}), and the turnover frequency (TOF) were calculated using the following equations:

$$\mathscr{X}_{CO_2}(\%) = \frac{F_{CO_2\ (in)} - F_{CO_2\ (out)}}{F_{CO_2\ (in)}} \times 100\% \quad (5)$$

$$S_{MeOH}(\%) = \frac{F_{MeOH}}{F_{CO} + F_{MeOH}} \times 100\% \quad (6)$$

$$S_{CO}(\%) = \frac{F_{CO}}{F_{CO} + F_{MeOH}} \times 100\% \quad (7)$$

$$TOF_{Cu}\ (h^{-1}) = \frac{F_{MeOH}}{m_{cat} \bullet Cu^0{}_{sites}} \quad (8)$$

$$STY_{MeOH}(g_{MeOH} \bullet g_{cat}{}^{-1} h^{-1}) = \frac{F_{MeOH} MW_{MeOH}}{m_{cat}} \quad (9)$$

Where $F_{CO2(in)}$ and $F_{CO2(out)}$ represent the inlet and outlet molar flows of CO_2, F_{MeOH} is the outlet molar flow of methanol, F_{CO} is the outlet molar flow of CO, MW_{MeOH} is the molar weight of methanol, m_{cat} is the mass of catalyst charged in the reactor and Cu^0_{sites} is the number of Cu^0 exposed active sites.

3. Results and discussion

3.1. Chemical and structural characterization

The ICP-MS elemental composition analysis (Table 1) confirmed the presence of magnesium in both promoted synthesized catalysts (0.8 wt% for CZAM_2 and 2.6 wt% for CZAM_5), thereby supporting the effectiveness of co-precipitation as a synthesis method, and in the commercial catalyst (1.4 wt%), analysed for comparison purposes. Synthesized catalysts were analysed after calcination. Table 1 also reports the mass ratio between Cu and Zn. A slight fluctuation can be observed, particularly in sample CZAM_5, which is likely attributable to variations in pH and temperature during the synthesis process. In fact, these parameters are known to significantly influence the outcome of coprecipitation synthesis applied for CZA systems [60].

The surface areas determined using the Brunauer-Emmett-Teller (BET) method, are reported in Table 1. It was observed that increasing the amount of magnesium in the catalysts produced an increase in the BET surface area, with values of 72, 84, 94, and 109 $m^2 \cdot g^{-1}$. The progressive rise in surface area follows the order CZA < CZAM_2 < Commercial Catalyst < CZAM_5, which is consistent with the increasing concentration of the promoter in each sample (0 wt%, 0.8 wt%, 1.4 wt% and 2.6 wt% respectively). Recently, Wang et al. [55] prepared a very similar catalyst, CZA with 5 mol% of Mg, obtaining a BET surface area of 54.7 $m^2 \cdot g^{-1}$. The increase in CZA surface area due to Mg loadings has already been reported by Zhang et al. [51] and Ay et al. [54]. Such an effect has been observed in similar systems too; namely, Schumann et al. [44], increased the ZnO support area by simply introducing Mg. Also, Dasireddy et al. [34], showed that Cu/Mg/Al catalyst displayed a marked increase in the BET area compared to the Cu/Zn/Al catalyst.

The adsorption-desorption isotherms of N_2 obtained for the synthesized catalysts and the commercial catalyst reported in the Supporting Information (Figure S1) show that all samples are mesoporous, exhibiting a Type IV isotherm. The pore volumes, calculated with the BJH method based on the desorption branch (Figure S2), exhibit a very different profile among all catalysts. The commercial catalysts, CZA and CZAM_2, show peaks with smaller pore widths, which shift as the amount of Mg in the catalyst increases. However, all the synthesized catalysts (CZA, CZAM_2 and CZAM_5) display peaks at larger pore widths, which are not observed in the commercial catalyst.

The H_2-TPR analysis of calcined samples (Fig. 1) shows that all catalysts, synthesized and commercial, are completely reduced once 250 °C is reached. Additionally, an effect of Mg on the temperature of the maximum H_2 uptake is evident, showing a slight trend of increasing temperature with higher promoter concentration: 216 °C for CZA, 218 °C for commercial, 225 °C for CZAM_2, and 233 °C for CZAM_5. Since ZnO cannot be reduced below 600 °C [44,61], no peaks corresponding to this phase were observed. This result demonstrates that the addition of Mg seems to be unfavourable for the reduction of CuO. One possible explanation could lie in the reducibility of Mg itself, which, in the temperature range between 50 °C and 600 °C, does not take place [36]. Therefore, since it is not a reducible support, it does not improve

Table 1
Theoretical catalyst elemental composition (expected) compared with results from ICP-MS chemical analysis (measured), Cu/Zn wt% ratios, and BET surface area of calcined catalysts.

Sample	Concentration of metals (wt%)								Cu/Zn ratio	BET Surface Area($m^2 \cdot g^{-1}$)
	Expected				Measured					
	Cu	Zn	Al	Mg	Cu	Zn	Al	Mg		
Commercial*	-	-	-	-	66.1	25.4	7.1	1.4	2.6	94
CZA	68.0	29.1	2.9	0	68.8	28.4	2.8	0	2.4	72
CZAM_2	67.2	28.7	2.9	1.2	69.2	28.0	2.8	0.8	2.5	84
CZAM_5	66.0	28.2	2.8	2.9	63.5	30.7	3.2	2.6	2.1	109

* Traces of titanium were also found from the elemental analysis.

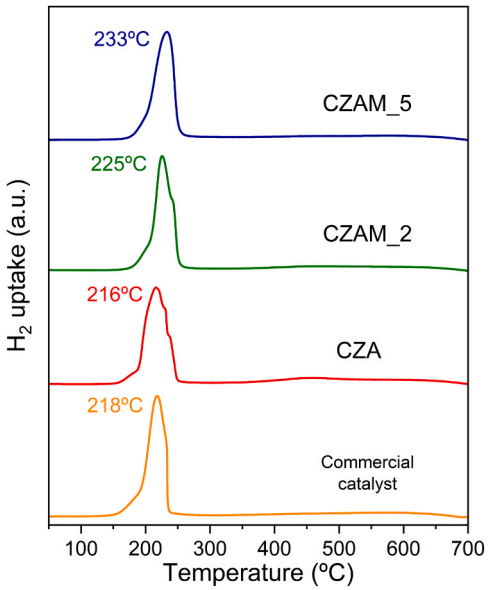

Fig. 1. H_2-TPR profiles of commercial and synthesized catalysts after calcination. Reported temperatures refer to the maximum of H_2 uptake.

the reducibility of the catalyst. The shift of the reduction peak to higher temperatures due to the presence of Mg is common in Cu-based catalysts. It has already been observed in Cu/ZnO by Schumann et al. [44] and Chen et al. [36], in Cu/ZrO/ZnO by He et al. [43], and specifically in $Cu/ZnO/Al_2O_3$ by Lee et al. [62] and Beiramar et al. [52]. On top of that, as the Mg concentration increases, a progressive decrease in the number of reduction peaks is observed: the CZA sample exhibits two shoulders that progressively decline and eventually vanish in the CZAM_5 sample. As reported in the literature [35], different peaks in Cu-based catalysts reduction profiles are usually associated with different aggregation states of CuO, Cu_2O, and/or their combination, representing Cu species with different reduction capabilities. Therefore, Mg seems to promote the formation of a single copper species during calcination; as its concentration increases, there is a progressive reduction in the peaks of the reduced species.

The dispersion of metallic copper, a key factor in CO_2 hydrogenation, was evaluated using both N_2O chemisorption and XRD analysis (Table 2). The N_2O chemisorption results indicate that Mg addition significantly enhances the accessible active surface area of copper. The CZAM_5 catalyst exhibits the highest dispersion (**9.8 %**) and active surface area (41.8 $m^2 \cdot g^{-1}$), followed closely by the commercial catalyst (**9.0 %**) and CZAM_2 (**8.4 %**). In contrast, the undoped CZA shows poor dispersion (**3.7 %**), correlating with its lower catalytic performance.

XRD-derived dispersions corroborate this trend, with CZAM_5 presenting the smallest Cu crystallite size (4.6 nm) and the highest calculated dispersion. These results demonstrate that Mg acts as a structural promoter, preventing copper sintering and promoting better metal dispersion.

Table 2
Summary of Cu^0 phase dispersion and surface area determined by N_2O chemisorption analysis, and Cu^0 dispersion and crystallite sizes determined by XRD. All data refers to the reduced catalysts.

Sample	N_2O Chemisorption			X-ray diffraction	
	D_{Cu} (%)	Cu^0 Sites (mol_{Cu}/g_{cat})	S_area Cu^0 (m^2_{Cu}/g_{cat})	D_{Cu} (%)	Cu^0 crystallite size (nm)
Commercial	9.0	$9.39 \cdot 10^{-4}$	39	46.7	5.6
CZA	3.7	$3.94 \cdot 10^{-4}$	16	23.0	11.7
CZAM_2	8.4	$8.87 \cdot 10^{-4}$	37	51.3	5.1
CZAM_5	9.8	$1.01 \cdot 10^{-3}$	42	56.8	4.6

The qualitative XRD analysis of the synthesized catalysts (Fig. 2) detected the formation of CuO following calcination, with a monoclinic phase and space group *C2/c* (Ref: 00–045–0937), and ZnO with a hexagonal phase and space group *P63mc* (Ref: 01–080–0075). The catalyst synthesized without promoter (CZA) shows a diffraction pattern with relatively higher and narrower peaks compared to the XRD profiles obtained from catalysts with MgO (CZAM_2, CZAM_5). In these samples, a noticeable reduction in the CuO phase peaks is observed, along with peak broadening. Peak broadening of the CuO phase is also observed in the XRD profile of the commercial catalyst, which, as shown by the ICP-MS analysis (Table 1), contains a 1.4 wt% of Mg. In further agreement with the elemental analysis results (Table 1), the commercial catalyst also exhibits an orthorhombic aluminium titanium oxide phase, with space group *Bbmm* (Ref: 01–070–1435).

No promoter diffraction peaks were detected, probably due to its very low content in all catalysts [52]. The reduced intensity and broadening of the CuO diffraction peaks upon the introduction of alkali metals, including Mg, have also been observed by Dasireddy et al. [34], who compared various Cu/MO/Al systems where MO is the promoter; by He et al. [43] in a Cu/ZrO/ZnO system promoted with Mg, and specifically, in CZA by Ay et al. [54]. The broadening of diffraction peaks indicates a decrease in the crystallinity of the sample due to the reduction in crystallite size. Therefore, it can be assumed that the addition of Mg promoted the reduction of CuO crystallites, as also observed by Chen et al. [36] in the preparation of a Cu/ZnO catalyst with Mg.

It is well known that a higher BET surface area can be achieved by a CuO phase with smaller crystallites [63,64]. Namely, Chen et al. [36] observed that the addition of small amounts of Mg increased the specific BET area and simultaneously decreased CuO crystallite size. In our case, a clear trend was observed across all samples linking MgO loading to structural properties. As Mg content increases, the BET surface area of the calcined catalysts rises steadily (Table 1), likely due to better control over crystallite growth and particle agglomeration. This is consistent with the observed decrease in Cu crystallite size determined by XRD. In parallel, metallic copper surface area and Cu^0 dispersion, quantified via N_2O chemisorption, increase accordingly (Table 2). The CZAM_5 catalyst, with the highest Mg content (2.6 wt%), shows the largest BET area (109 $m^2 \cdot g^{-1}$), the smallest Cu crystallites (4.6 nm), and the highest Cu dispersion (**9.8 %**). These results confirm the dual role of MgO in enhancing both the textural and catalytic surface properties of CZA-based materials.

The crystallinity progression detected in calcined catalysts can also be observed in XRD patterns of samples reduced at 250 ºC in the reaction

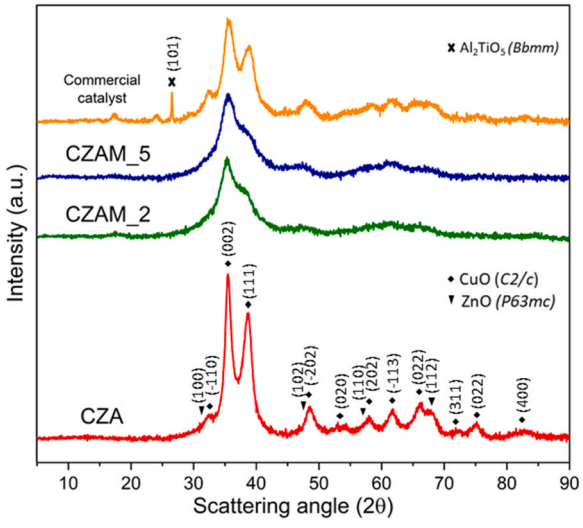

Fig. 2. XRD patterns of commercial and synthesized catalysts after calcination.

chamber (Fig. 3a). The synthesized catalysts were compared with the commercial catalysts. After reduction, the catalyst without a promoter (CZA) maintains a profile with relatively higher and narrower peaks, followed by the two promoted catalysts (CZAM_2 and CZAM_5), which instead clearly exhibit peak broadening. In all cases, the presence of metallic Cu with a cubic phase (Ref: 01–085–1326, space group: *Fm3m*) and ZnO with a hexagonal phase (Ref: 01–080–0075, space group: *P63mc*) was qualitatively identified. The detection of only Cu and ZnO phases suggests that CuO was entirely converted to Cu^0 during the reduction process. The Cu^0 phase crystallite sizes, calculated for all catalysts using the Scherrer equation applied to the diffraction peak at 43° in 2 theta, are shown in Table 2 and reflect the previous crystallinity trend observed in calcined catalysts. The increasing presence of Mg in the synthesized catalysts seems to reduce the crystallite size of the catalyst's active phase, metallic Cu. CZAM_2 and CZAM_5 indeed show significantly smaller crystallite sizes, 5.1 nm and 4.6 nm respectively, compared to the pure CZA catalyst (11.7 nm). For comparison, the commercial catalyst with Mg also exhibits a smaller Cu crystallite size, with a value comparable to that of the synthesized samples (5.6 nm). A similar result (5.31 nm of crystallite size) was also reported by Ay et al. [54] in a $Cu/ZnO/Al_2O_3$ catalyst promoted with Mg. The influence of Mg on XRD profiles was also studied by Cheng et al. in Mg-promoted CZA [48]; as the Mg concentration increased, a continuous broadening of the characteristic Cu peaks was observed, indicating a decrease in Cu crystallite size, thus suggesting the role of magnesium in the dispersion of Cu. As reported in the literature [63,64], the formation of smaller Cu crystallite sizes also seems to indicate a high dispersion of Cu in the catalyst.

Additionally, XRD analysis was performed on the spent catalysts (Fig. 3b) to investigate structural changes induced by the reaction, after their separation from the SiC used in the catalytic bed. As can be observed, a monoclinic CuO phase (Ref: 00–045–0937) with space group *C2/c* is present in both the commercial and the synthesized CZA catalysts, which was not detected in the reduced samples (Fig. 3a). Thus, part of the metallic Cu appears to have been oxidized during the reaction. However, this phase is not observed in the catalysts synthesized with Mg (CZAM_2 and CZAM_5). In all cases, the metallic Cu (Ref: 01–085–1326) and the same ZnO phase (Ref: 01–080–0075) found in the reduced samples (Fig. 3a) remain. Only for CZAM_5, likely due to the high concentration of Mg in this catalyst, a magnesium carbonate phase (Ref: 01–080–0101) is formed. The Scherrer equation was applied to the diffraction peak at $2\theta = 43°$ to estimate the crystallite sizes of Cu^0 phase in the spent catalysts. The calculated sizes were 9.0 nm for the commercial catalyst, 19.0 nm for CZA, 9.2 nm for CZAM_2, and 8.8 nm for CZAM_5. Compared to the values obtained for the fresh catalysts (Table 2), the spent catalysts exhibited a significant increase in the crystallite size of the Cu^0 phase, with values approximately doubling in all cases. This growth in crystallite size is well-known for CZA-based catalysts [26] and is attributed to the phenomenon of sintering, i.e., the aggregation and enlargement of the active phase particles as a result of the reaction, particularly promoted by the water as a by-product of the RWGS.

The surface basicity of the prepared catalysts was evaluated by CO_2 temperature-programmed desorption (CO_2-TPD). The experiments were conducted after catalyst reduction under H_2/Ar flow, followed by CO_2 adsorption at 50 °C. The desorption was performed under helium flow with a heating rate of 10 °C·min^{-1}, up to 800 °C. The desorbed species were monitored using both a thermal conductivity detector (TCD) and a mass spectrometer (MS) to ensure accurate identification of CO_2 release. Fig. 4a shows the CO_2-TPD profiles of the CZA, CZAM_2, CZAM_5, and the commercial catalyst.

All samples exhibit characteristic desorption peaks corresponding to weak, moderate, and strong basic sites, typically associated with surface hydroxyls, metal-oxygen pairs, and low-coordinated oxygen anions, respectively.

The undoped CZA catalyst displays the lowest overall desorption intensity, indicating a limited number of basic sites. Upon Mg incorporation, a clear increase in both the intensity and the temperature of desorption peaks is observed. The CZAM_2 sample (2 wt% MgO) shows a significant enhancement of moderate basic sites, while the CZAM_5 catalyst (5 wt% MgO) exhibits a pronounced desorption at higher temperatures, revealing the formation of strong basic sites. Interestingly, the commercial catalyst presents a desorption pattern dominated by moderate basic sites, with negligible contribution from strong basic sites, which aligns with its optimized industrial formulation aimed at balancing CO_2 activation and product selectivity.

To confirm that the detected desorption signals correspond exclusively to CO_2, MS monitoring of $m/z = 44$ was performed throughout the TPD experiments. Results are shown in Fig. 4b.

Additional tracking of $m/z = 18$ (H_2O) and $m/z = 28$ (CO/N_2) showed no significant desorption of other species, validating that the profiles obtained reflect true CO_2 desorption (see Supporting Information, Figure S5).

These results demonstrate that Mg addition effectively increases the basicity of CZA catalysts, but excessive loading leads to a predominance of strong basic sites, which, as discussed below, impacts catalytic performance by promoting side reactions such as the RWGS reaction.

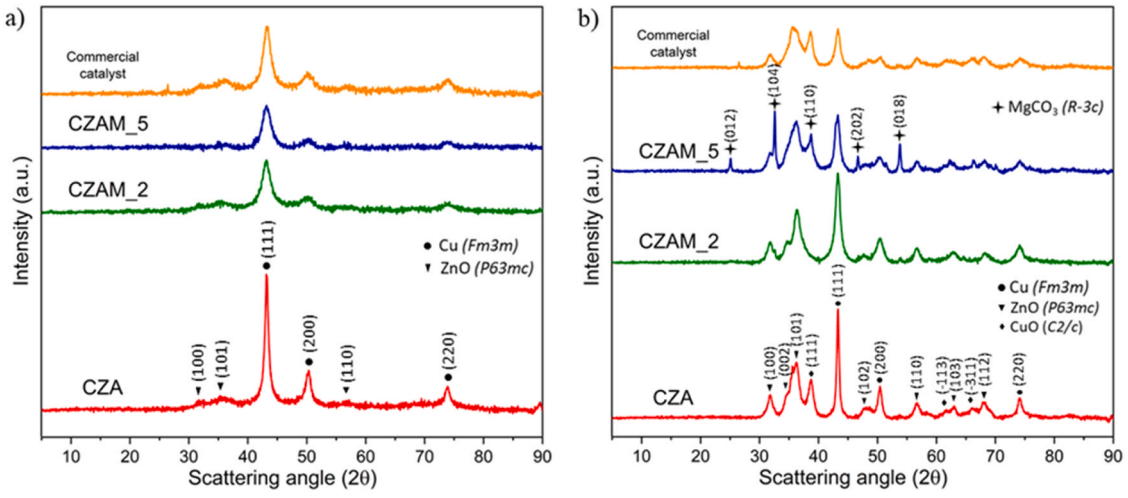

Fig. 3. XRD patterns of (a) fresh catalysts reduced at 250 °C under an H_2/N_2 flow in the reaction chamber and (b) spent catalysts, after 49 h of reaction at 240 °C and 50 bar.

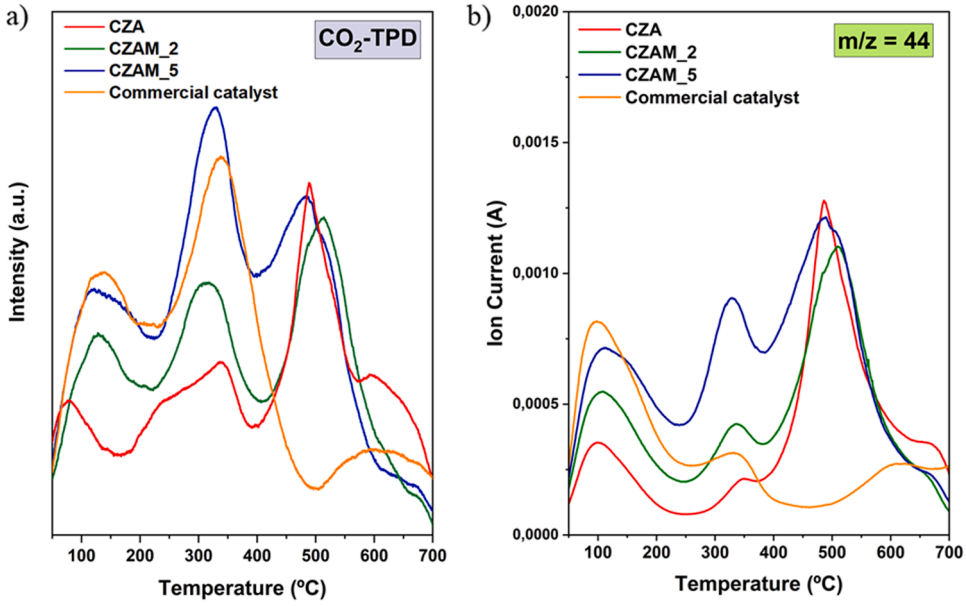

Fig. 4. (a) CO_2-TPD profiles of the CZA, CZAM_2, CZAM_5, and the commercial catalyst and (b) MS monitoring of $m/z = 44$ obtained during CO_2-TPD analysis.

3.2. Catalytic activity

The CO_2 conversion for synthesized and commercial catalysts, as a function of TOS and increasing GHSV, is shown in Fig. 5. It can be observed that the presence of Mg consistently improves the CO_2 conversion, with catalysts containing the promoter (CZAM_2, CZAM_5, and the commercial catalyst) always exhibiting higher conversion values for each GHSV. The catalyst with an intermediate Mg concentration, CZAM_2, shows a conversion most similar to the commercial catalyst and is the best among the synthesized ones. For all samples, a significant influence of GHSV on CO_2 conversion is observed, with conversion decreasing substantially as GHSV increases. The highest conversion values, therefore, correspond to the lowest GHSV ($2500h^{-1}$) for all catalysts. During the final seven hours of the reaction, when the initial GHSV was restored, it can be noted that all catalysts returned to their initial conversion values, indicating that no significant deactivation of the catalyst occurred under these conditions.

The selectivity (%) to methanol (MeOH) and carbon monoxide (CO) is shown in Fig. 6. For all catalysts and under all GHSV conditions used, the carbon balance (Figure S2), calculated by considering MeOH and CO as the only products, is always greater than 91 %. Therefore, selectivity was calculated by considering only these two products. In this case, for GHSV values between $2500h^{-1}$ and $7500h^{-1}$, it can be observed that the highest methanol selectivity corresponds to CZAM_2, among the synthesized catalysts. For intermediate-to-high GHSV values, ranging from $10000h^{-1}$ to $15000h^{-1}$, the CZA catalyst shows the highest methanol selectivity among the synthesized catalysts. On the other hand, the CZAM_5 catalyst exhibits the lowest methanol selectivity across all GHSV conditions. In this case as well, for all the catalysts, a return to the initial selectivity values is observed during the last seven hours of the reaction, when the initial GHSV condition ($2500h^{-1}$) was restored.

The Space Time Yield (STY) to methanol, as a function of TOS, is shown in Fig. 7a. Once again, it can be observed that the catalyst with an intermediate concentration of the promoter, CZAM_2, shows the most similar profile to the commercial catalyst. Of course, according to the outlet methanol flow (Eq. (9)), productivity (STY) increases with the

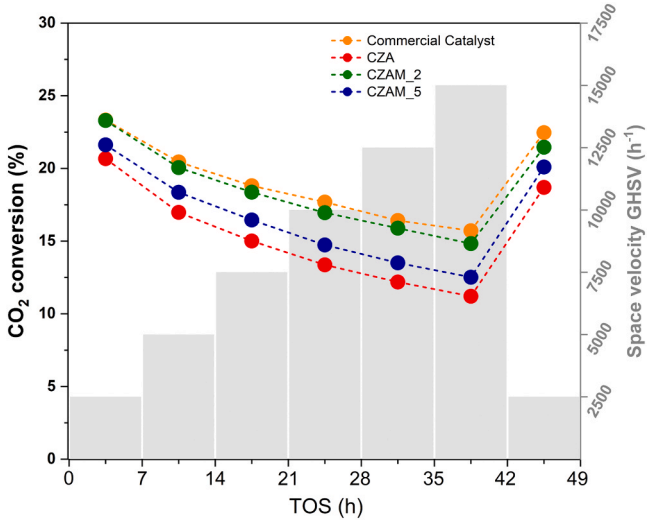

Fig. 5. Average values of CO_2 conversion for all catalysts, in each GHSV condition, during 49 h of reaction at 240 °C and 50 bar.

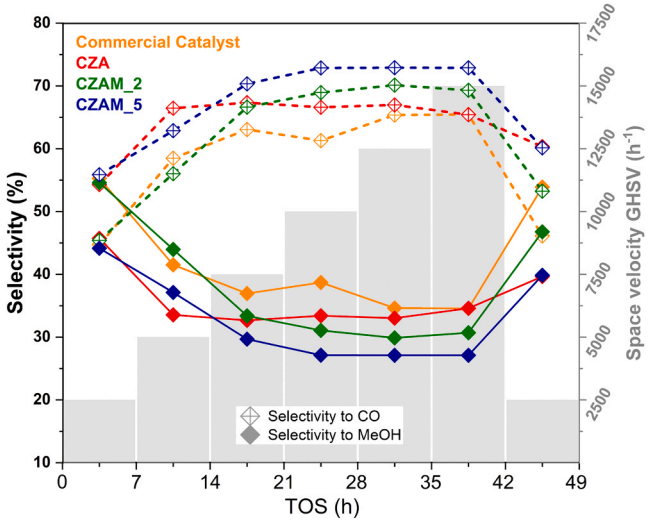

Fig. 6. Average values of CO and methanol selectivity for all catalysts, in each GHSV condition, during 49 h of reaction at 240 °C and 50 bar.

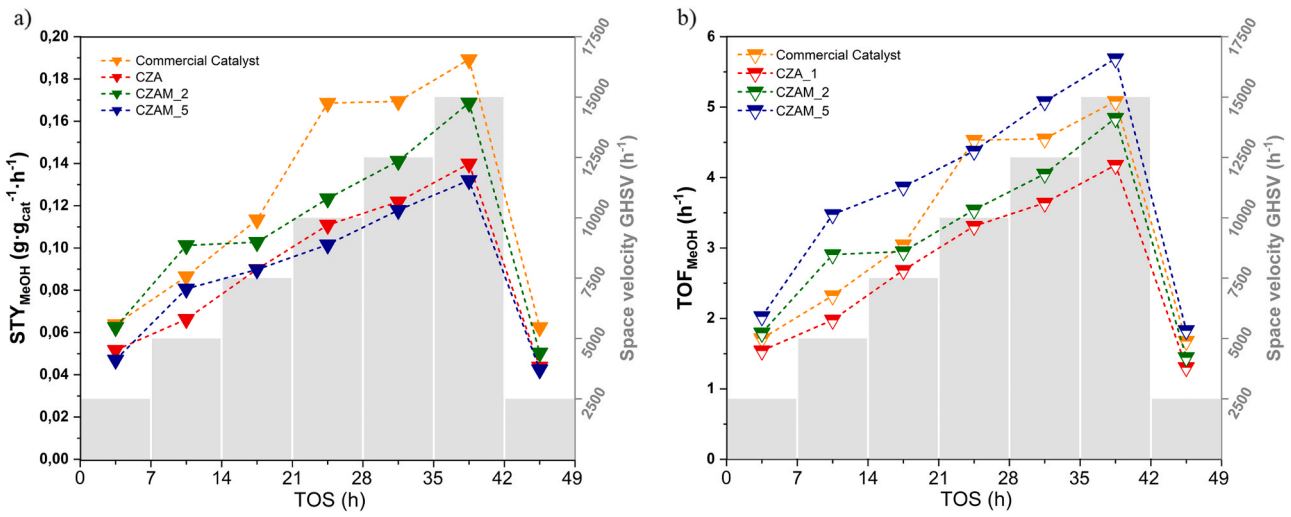

Fig. 7. Average values of methanol STY (a) and methanol TOF (b) for all catalysts, in each GHSV condition, during 49 h of reaction at 240 °C and 50 bar.

GHSV, but it can be observed that under each step of GHSV conditions, the CZAM_2 catalyst demonstrates the best productivity among all synthesized catalysts. Furthermore, these results indicate that the catalyst with the highest Mg concentration, CZAM_5, exhibits the lowest productivity. However, this changes when considering the methanol TOF (Fig. 7b): while the CZA, CZAM_2, and commercial catalysts maintain their activity trend, the TOF of CZAM_5 increases significantly, actually exceeding the activity of all other catalysts. This result could suggest that the intrinsic activity of each CZAM_5 metallic Cu site, represented by the TOF, could be higher than the other catalyst sites. However, since CZAM_5 active sites are fewer in number (low number of Cu^0 sites and low Cu surface area compared to the other catalysts), as shown by the N_2O chemisorption (Table 2), they lead to a lower STY.

The combination of CO_2-TPD, H_2-TPR, XRD, BET, and catalytic testing highlights that Mg plays a dual role in CZA-based catalysts: it enhances surface basicity and promotes copper dispersion. However, despite CZAM_5 having the highest dispersion, its methanol selectivity is compromised due to the excessive surface basicity, as revealed by CO_2-TPD. This highlights that optimal catalytic performance arises from a balance between high copper dispersion and controlled basicity, as observed in CZAM_2 and the commercial catalyst. The role of Mg in enhancing surface basicity and copper dispersion has been previously reported to improve CO_2 adsorption and methanol selectivity in Cu-ZnO-based catalysts. However, excessive basicity can alter adsorption dynamics and promote side reactions if not properly controlled [40]. Our results align with these findings, demonstrating that a moderate Mg loading optimizes the balance between CO_2 activation and methanol selectivity.

Based on the previous results, it is evident that all catalysts exhibit improved CO_2 conversion and methanol selectivity at the lowest GHSV value, specifically $2500h^{-1}$. The STY and TOF for methanol obviously increase as the GHSV increases, since their estimation is directly proportional to the methanol flow produced (equations 8 and 9). Consequently, it is reasonable to state that a low GHSV improves the activity of the studied catalysts, a trend that has also been observed with the CZA catalyst for methanol synthesis [65]. The activity values for each catalyst at $2500h^{-1}$ conditions are reported in Table 3. Under the same conditions, the CZAM_2 catalyst achieved the highest CO_2 conversion, methanol selectivity, and STY.

A summary of the comparison of catalytic activity results for CO_2 conversion to methanol of CZAM_2 with other studies in the literature [48,54–57] is compiled in Table 4. CZAM_2 shows a high CO_2 conversion, while methanol selectivity remains moderate yet significant, in both cases close to the equilibrium values [66]. This behavior is pretty

Table 3
Activity for all catalysts, in 2500 h^{-1} GHSV conditions for the conversion of CO_2 to methanol at 240 °C and 50 bar.

Catalyst	CO_2 Conversion (%)	Methanol Selectivity (%)	Methanol STY ($g \cdot g_{cat}^{-1} h^{-1}$)	TOF (h^{-1})
Commercial	23.3	55	0.064	1.71
CZA	20.7	46	0.052	1.54
CZAM_2	23.3	55	0.062	1.80
CZAM_5	21.6	44	0.047	2.03

similar to the results obtained with the catalysts a) CuZnZr or b) a mixture of CZA and hydrotalcite (lines 3 and 4 in Table 4). However, the comparison with other results published in the literature is complicated because they use lower temperature reactions (line 5 in Table 4) or conversion level (lines 4 and 5, in Table 4). Lower temperature favors higher selectivity but low activity, and different conversion level will affect the catalyst performance. Still, the behavior of the CZAM_2 shows a very good performance.

The good catalytic activity exhibited by CZAM_2 encouraged us to perform a stability test, conducted under the same conditions as the previous reactions (240 °C, 50 bar, CO_2/H_2: 1/3) for 120 h (Fig. 8). The CO_2 conversion dropped for a short TOS from an initial value of 26–21 % after 60 h, remaining stable for a long time on stream. Methanol selectivity, initially at 50 %, reduced to 41 % in short TOS, also becoming more stable over longer times. The STY, on the other hand, decreased slightly from an initial value of 0.052 $g_{MeOH} \cdot g_{cat} \cdot h^{-1}$ to 0.045 $g_{MeOH} \cdot g_{cat} \cdot h^{-1}$, showing a stable trend for longer TOS. A similar stability study (120 h) was conducted by Wang et al. [55] investigated the conversion of CO_2 to methanol using a similar $Cu/ZnO/Al_2O_3/MgO$ catalyst. Although the reaction occurred at a lower temperature and achieved a CO_2 conversion of only 9.4 %, the catalyst remained stable under these conditions.

The CZAM_2 catalyst (2 wt% MgO) achieves the optimal balance, showing high CO_2 conversion, methanol selectivity, and remarkable stability over 120 h of reaction, making it a promising candidate for industrial CO_2 hydrogenation to methanol.

Therefore, while Mg improves copper dispersion, excessive loading leads to undesirable shifts in reaction selectivity, reinforcing the importance of fine-tuning both physicochemical properties for efficient CO_2 hydrogenation to methanol. In Fig. 9, we explored the correlation between Cu dispersion and methanol selectivity.

As shown in Fig. 9, the relationship between these two parameters is not linear. While Mg addition clearly enhances copper dispersion from

Table 4
Catalytic activity of CZAM_2 catalyst at 2500 h^{-1} of GHSV, compared with other copper-based catalysts from literature studies used for conversion of CO_2 to methanol.

Catalyst	H_2/CO_2 ratio	T (°C)	P (MPa)	GHSV (h^{-1})	CO_2 Conversion (%)	Methanol Selectivity (%)	REF
CZAL (L: La 2.3 mol%)	3/1	260	5.0	16000	20.0	72	[67]
CuZnZr-CP (6/3/1)	3/1	250	5.0	3000*	26.5	52	[68]
CZA-H40 (40 % hydrotalcite)	3/1	250	3.0	2600*	6.0	73	[66]
CZAS (S: Si 0.3)	–	250	3.0	6000*	12.6	85	[59]
CZAM (M: Mg 5 mol%)	3/1	190	3.0	10000	9.4	80	
CZAM (M: Mg 3.5 mol%)	3/1	240	5.0	2500	23.3	55	This work

* GHSV expressed in $mL \cdot g^{-1} \cdot h^{-1}$. All other values refer to h^{-1}.

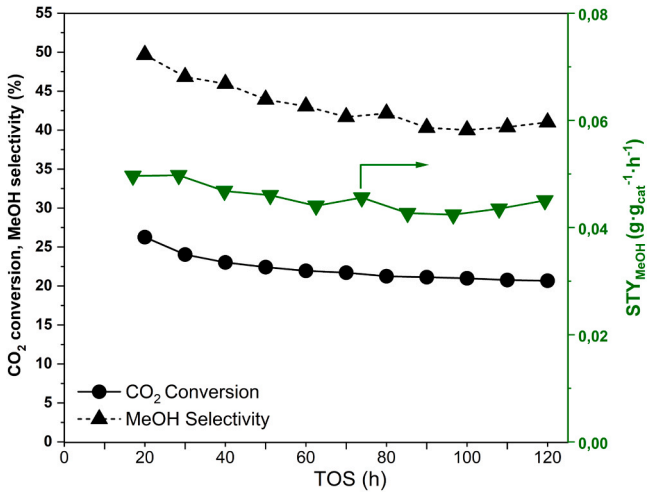

Fig. 8. Stability test of CZAM_2 catalyst, conducted for 120 h at 240 °C, 50 bar and 2500 h^{-1}.

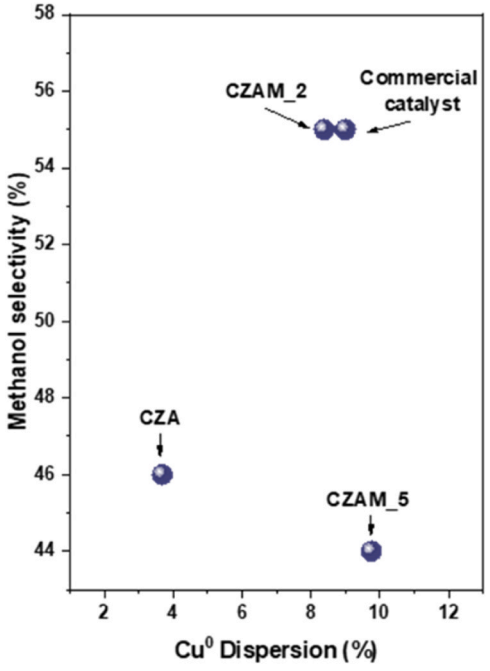

Fig. 9. Correlation between Cu^0 dispersion (N_2O chemisorption) and methanol selectivity for the studied catalysts.

3.7 % in CZA to **9.8 %** in CZAM_5, this increase does not directly translate into higher methanol selectivity. In fact, the CZAM_5 catalyst, despite exhibiting the highest Cu dispersion, shows the lowest methanol selectivity due to the excessive formation of strong basic sites, as evidenced by CO_2-TPD analysis. These sites promote side reactions, particularly the reverse water-gas shift (RWGS), leading to higher CO production.

Conversely, both CZAM_2 and the commercial catalyst achieve the best methanol selectivity (≈ **55 %**) at intermediate dispersion values (≈ 8 – **9 %**). This indicates that optimal catalytic behaviour arises from a balance between adequate copper dispersion, ensuring a sufficient number of active sites, and controlled surface basicity, which favours CO_2 activation without promoting undesired pathways.

These findings highlight that maximizing dispersion alone is not sufficient; instead, careful tuning of both structural and surface chemical properties is essential to enhance selectivity in CO_2 hydrogenation to methanol.

4. Conclusions

In this study, we investigated the influence of magnesium loadings on the structure and activity of copper-based catalysts for the conversion of CO_2 to methanol. The overall results indicate that magnesium acts as a promoter, significantly affecting both the structure and activity of the studied catalysts. ICP-MS analysis confirmed the presence of magnesium in the co-precipitated and calcined samples (CZAM_2 and CZAM_5). XRD analysis, N_2 adsorption-desorption isotherms and CO_2-TPD analysis revealed respectively a decrease in crystallite size, an increase in BET surface area and in metallic Cu phase dispersion as the magnesium concentration increased. A clear relationship was established between MgO loading and the structural properties of the catalysts: the incorporation of magnesium led to a progressive increase in BET surface area, from 72 $m^2 \cdot g^{-1}$ in the undoped CZA catalyst to 109 $m^2 \cdot g^{-1}$ in CZAM_5. This effect was accompanied by a reduction in Cu crystallite size and a corresponding enhancement of metallic copper surface area and Cu^0 dispersion, as confirmed by both XRD and N_2O chemisorption analyses. These findings confirm that MgO acts as a structural promoter, improving the dispersion and accessibility of Cu^0 active sites.

However, excessive magnesium concentration (CZAM_5) appears to hinder CO_2 conversion and methanol selectivity. In this context, the pronounced formation of strong basic sites appears to be a key factor, as it promotes secondary reactions leading to increased CO selectivity. Otherwise, the intrinsic activity, as indicated by the TOF, seems to be better for CZAM_5, suggesting that each of its fewer reaction sites exhibited higher catalytic activity. The CZAM_2 catalyst, with an intermediate magnesium concentration (0.8 wt%), revealed the best overall performance, showing a small crystallite size (5.1 nm) and a significant increase in BET surface area (84 $m^2 \cdot g^{-1}$) and copper dispersion (8.4 %) compared to the catalyst without a promoter (CZA).

The catalytic activity of CZAM_2, considering CO_2 conversion, methanol selectivity, and Space-Time Yield (STY), was the closest to that of the commercial catalyst. The effect of GHSV was also investigated, showing that low GHSV optimizes catalytic activity for all catalysts, increasing CO_2 conversion and methanol selectivity. In particular, the CZAM_2 catalyst showed the best results at 2500 h^{-1}, showing a CO_2 conversion of 23.3 %, significantly higher than the average reported in the literature for Cu-based modified catalysts used in this specific reaction, and a good methanol selectivity of 55 %. The slight decrease in CO_2 conversion (from 26–21 %) and methanol selectivity (from 50 % to 41 %), during a 120-hour stability test, confirms that CZAM_2 is able to sustain a good activity over time. While three MgO loadings (0, 2, and 5 wt%) were analysed in this study to elucidate the main trends of promotion effects, future work could include intermediate compositions to achieve a finer optimization of the MgO content in CZA-based catalysts. The overall results of this study suggest that an optimal concentration of magnesium as a promoter for copper-based catalysts (0.8 wt% in our case) is crucial to improve catalytic performance and that GHSV control is essential to optimize catalytic activity in the conversion of CO_2 to methanol.

CRediT authorship contribution statement

Silvia Morales-delaRosa: Writing – review & editing, Supervision, Resources, Project administration, Methodology, Funding acquisition, Formal analysis, Conceptualization. **Dalia Liuzzi:** Writing – review & editing, Supervision, Methodology. **Cristina Peinado:** Writing – review & editing, Methodology, Formal analysis. **Maria Dore:** Writing – original draft, Investigation, Formal analysis. **Jose M. Campos-Martin:** Writing – review & editing, Resources, Methodology, Conceptualization. **Sergio Rojas:** Writing – review & editing, Resources.

Declaration of Competing Interest

The authors declare that they have no known competing financial interests or personal relationships that could have appeared to influence the work reported in this paper.

Acknowledgements

The research work has been developed in the frame of the FUELPHORIA project, funded by the European Union's Horizon Europe research and innovation program under Grant Agreement number 101118286 and it was supported by MCIN with funding from NextGenerationEU (PRTR-C17.I1) within the Planes Complementarios con CCAA (Area of Green Hydrogen and Energy) and it has been carried out in the CSIC Interdisciplinary Thematic Platform (PTI+) Transición Energética Sostenible+ (PTI-TRANSENER+). The authors acknowledge support of the publication fee by the CSIC Open Access Publication Support Initiative through its Unit of Information Resources for Research (URICI).

Appendix A. Supporting information

Supplementary data associated with this article can be found in the online version at doi:10.1016/j.cattod.2025.115425

Data availability

Data will be made available on request.

References

[1] J.U. Ahmed, Editorial Author information, BIRDEM Med J. 14 (2024) 61–64, https://doi.org/10.3329/birdem.v14i2.73299.
[2] C. Dupont, B. Moore, E.L. Boasson, V. Gravey, A. Jordan, P. Kivimaa, K. Kulovesi, C. Kuzemko, S. Oberthür, D. Panchuk, J. Rosamond, D. Torney, J. Tosun, I. von Homeyer, Three decades of EU climate policy: Racing toward climate neutrality? Wiley Inter. Rev. Clim. Change 15 (2024) https://doi.org/10.1002/wcc.863.
[3] B. Gavurova, M. Rigelsky, V. Ivankova, Greenhouse gas emissions and health in the countries of the European Union, Front Public Health 9 (2021), https://doi.org/10.3389/fpubh.2021.756652.
[4] J.E. Duggan, Recent progress in sustainable energy systems development: investment, operations, and decarbonization, Curr. Sustain. /Renew. Energy Rep. 12 (1) (2025), https://doi.org/10.1007/s40518-024-00248-3.
[5] F. Nath, M.N. Mahmood, N. Yousuf, Recent advances in CCUS: a critical review on technologies, regulatory aspects and economics, Geoenergy Sci. Eng. 238 (2024), https://doi.org/10.1016/j.geoen.2024.212726.
[6] M. Ozkan, A.A. Akhavi, W.C. Coley, R. Shang, Y. Ma, Progress in carbon dioxide capture materials for deep decarbonization, Chem 8 (2022) 141–173, https://doi.org/10.1016/j.chempr.2021.12.013.
[7] C.B. Peres, P.M.R. Resende, L.J.R. Nunes, L.C.de Morais, Advances in Carbon Capture and Use (CCU) technologies: a comprehensive review and CO2 mitigation potential analysis, Clean. Technol. 4 (2022) 1193–1207, https://doi.org/10.3390/cleantechnol4040073.
[8] I. Onyedika, E. Wags, N. Digitemie[2], Carbon Capture and Utilization (CCU): a review of emerging applications and challenges, Eng. Sci. Technol. J. 5 (2024), https://doi.org/10.51594/estj/v5i3.949.
[9] J. Zhong, X. Yang, Z. Wu, B. Liang, Y. Huang, T. Zhang, State of the art and perspectives in heterogeneous catalysis of CO2 hydrogenation to methanol, Chem. Soc. Rev. 49 (2020) 1385–1413, https://doi.org/10.1039/c9cs00614a.
[10] M. Bertau, H. Offermanns, L. Plass, F. Schmidt, H.-J. Wernicke, in: Methanol: The Basic Chemical and Energy Feedstock of the Future, First Edition, Springer, Berlin, Heidelberg, 2014, https://doi.org/10.1007/978-3-642-39709-7.
[11] M.H. Mat Yasin, T. Yusaf, R. Mamat, A. Fitri Yusop, Characterization of a diesel engine operating with a small proportion of methanol as a fuel additive in biodiesel blend, Appl. Energy 114 (2014) 865–873, https://doi.org/10.1016/J.APENERGY.2013.06.012.
[12] K.A. Ali, A.Z. Abdullah, A.R. Mohamed, Recent development in catalytic technologies for methanol synthesis from renewable sources: a critical review, Renew. Sustain. Energy Rev. 44 (2015) 508–518, https://doi.org/10.1016/j.rser.2015.01.010.
[13] R. Laursen, D. Sofiadi, A. Bureau, Potential of Synthetic Fuels for Shipping Authors: Legal notice: Copyright notice 1, 2024. www.emsa.europa.eu.
[14] 2023, liorpt, European Maritime Safety Agency BUNKERING OF BIOFUELS IN MARITIME: CHARACTERISTICS, REGULATORY LANDSCAPE, AND SAFETY ASSESSMENT SAFE BUNKERING OF BIOFUELS. www.emsa.europa.eu.
[15] G.A. Olah, A. Goeppert, G.K.S. Prakash. Beyond Oil and Gas: The Methanol Economy, Third Edition, Wiley-VCH, 2018.
[16] S.S. Tabibian, M. Sharifzadeh, Statistical and analytical investigation of methanol applications, production technologies, value-chain and economy with a special focus on renewable methanol, Renew. Sustain. Energy Rev. 179 (2023), https://doi.org/10.1016/j.rser.2023.113281.
[17] P. Gao, F. Li, N. Zhao, F. Xiao, W. Wei, L. Zhong, Y. Sun, Influence of modifier (Mn, La, Ce, Zr and Y) on the performance of Cu/Zn/Al catalysts via hydrotalcite-like precursors for CO2 hydrogenation to methanol, Appl. Catal. A Gen. 468 (2013) 442–452, https://doi.org/10.1016/J.APCATA.2013.09.026.
[18] D. Allam, S. Bennici, L. Limousy, S. Hocine, Improved Cu- and Zn-based catalysts for CO2 hydrogenation to methanol, Comptes Rendus Chim. 22 (2019) 227–237, https://doi.org/10.1016/J.CRCI.2019.01.002.
[19] M. Sadeghinia, M. Rezaei, A. Nemati Kharat, M. Namayandeh Jorabchi, B. Nematollahi, F. Zareiekordshouli, Effect of In2O3 on the structural properties and catalytic performance of the CuO/ZnO/Al2O3 catalyst in CO2 and CO hydrogenation to methanol, Mol. Catal. 484 (2020) 110776, https://doi.org/10.1016/J.MCAT.2020.110776.
[20] A. Beck, M.A. Newton, L.G.A. van de Water, J.A. van Bokhoven, The Enigma of Methanol Synthesis by Cu/ZnO/Al2O3-Based Catalysts, Chem. Rev. 124 (2024) 4543–4678, https://doi.org/10.1021/acs.chemrev.3c00148.
[21] P. Sharma, J. Sebastian, S. Ghosh, D. Creaser, L. Olsson, Catalysis science & technology MINI REVIEW recent advances in hydrogenation of CO 2 into hydrocarbons via methanol intermediate over heterogeneous catalysts, Cite This Catal. Sci. Technol. 11 (2021) 1665, https://doi.org/10.1039/d0cy01913e.
[22] F. Meshkini, M. Taghizadeh, M. Bahmani, Investigating the effect of metal oxide additives on the properties of Cu/ZnO/Al2O3 catalysts in methanol synthesis from syngas using factorial experimental design, Fuel 89 (2010) 170–175, https://doi.org/10.1016/J.FUEL.2009.07.007.
[23] H. Zhang, C. Han, C. Li, P. Wang, H. Huang, S. Wang, J. Li, Design of Cu/ZnO/Al2O3 catalysts with a rich Cu-ZnO interface for enhanced CO2 hydrogenation to methanol using zinc-malachite as the precursor, N. J. Chem. 47 (2023) 5885–5893, https://doi.org/10.1039/d2nj05903g.
[24] S. Kanuri, S. Roy, C. Chakraborty, S.P. Datta, S.A. Singh, S. Dinda, An insight of CO2 hydrogenation to methanol synthesis: thermodynamics, catalysts, operating parameters, and reaction mechanism, Int. J. Energy Res 46 (2022) 5503–5522, https://doi.org/10.1002/er.7562.
[25] Y.F. Shi, S. Ma, Z.P. Liu, Copper-based catalysts for CO2 hydrogenation: a perspective on active sites, EES Catal. 1 (2023) 921–933, https://doi.org/10.1039/d3ey00152k.
[26] Y. Bielik, 2024, How Can the Water Tolerance of the Industrial Cu/ZnO/Al 2 O 3 Catalyst Used in Methanol Synthesis From CO 2 Be Enhanced?.
[27] M. Campanati, G. Fornasari, A. Vaccari, 2003, Fundamentals in the preparation of heterogeneous catalysts.
[28] C. Baltes, S. Vukojević, F. Schüth, Correlations between synthesis, precursor, and catalyst structure and activity of a large set of CuO/ZnO/Al2O3 catalysts for

methanol synthesis, J. Catal. 258 (2008) 334–344, https://doi.org/10.1016/J.JCAT.2008.07.004.
[29] M. Behrens, Coprecipitation: An excellent tool for the synthesis of supported metal catalysts – From the understanding of the well known recipes to new materials, Catal. Today 246 (2015) 46–54, https://doi.org/10.1016/J.CATTOD.2014.07.050.
[30] D. Liuzzi, C. Peinado, M.A. Peña, J. Van Kampen, J. Boon, S. Rojas, Increasing dimethyl ether production from biomass-derived syngas via sorption enhanced dimethyl ether synthesis, Sustain Energy Fuels 4 (2020) 5674–5681, https://doi.org/10.1039/D0SE01172J.
[31] C. Peinado, D. Liuzzi, A. Sanchís, L. Pascual, M.A. Peña, J. Boon, S. Rojas, In situ conditioning of CO2-rich syngas during the synthesis of methanol, Catalysts 11 (2021), https://doi.org/10.3390/catal11050534.
[32] L. Angelo, K. Kobl, L.M.M. Tejada, Y. Zimmermann, K. Parkhomenko, A.C. Roger, Study of CuZn MOx oxides (M = Al, Zr, Ce, CeZr) for the catalytic hydrogenation of CO2 into methanol, Comptes Rendus Chim. 18 (2015) 250–260, https://doi.org/10.1016/J.CRCI.2015.01.001/.
[33] T.P. Maniecki, P. Mierczyński, W. Maniukiewicz, D. Gebauer, W.K. Jozwiak, The effect of spinel type support FeAlO3, ZnAl2O 4, CrAl3O6 on physicochemical properties of Cu, Ag, Au, Ru supported catalysts for methanol synthesis, Kinet. Catal. 50 (2009) 228–234, https://doi.org/10.1134/S0023158409020128/METRICS.
[34] V.D.B.C. Dasireddy, N.S. Štefančič, M. Huš, B. Likozar, Effect of alkaline earth metal oxide (MO) Cu/MO/Al2O3 catalysts on methanol synthesis activity and selectivity via CO2 reduction, Fuel 233 (2018) 103–112, https://doi.org/10.1016/j.fuel.2018.06.046.
[35] V.D.B.C. Dasireddy, N.S. Štefančič, B. Likozar, Correlation between synthesis pH, structure and Cu/MgO/Al2O3 heterogeneous catalyst activity and selectivity in CO2 hydrogenation to methanol, J. CO2 Util. 28 (2018) 189–199, https://doi.org/10.1016/j.jcou.2018.09.002.
[36] F. Chen, W. Gao, K. Wang, C. Wang, X. Wu, N. Liu, X. Guo, Y. He, P. Zhang, G. Yang, N. Tsubaki, Enhanced performance and stability of Cu/ZnO catalyst by introducing MgO for low-temperature methanol synthesis using methanol itself as catalytic promoter, Fuel 315 (2022), https://doi.org/10.1016/j.fuel.2022.123272.
[37] G.C. Chinchen, K.C. Waugh, D.A. Whan, The activity and state of the copper surface in methanol synthesis catalysts, Appl. Catal. 25 (1986) 101–107, https://doi.org/10.1016/S0166-9834(00)81226-9.
[38] S. Golunski, R. Burch, CO2 Hydrogenation to Methanol over Copper Catalysts: Learning from Syngas Conversion, Top. Catal. 64 (2021) 974–983, https://doi.org/10.1007/s11244-021-01427-y.
[39] C. Peinado, D. Liuzzi, A. Sanchís, L. Pascual, M.A. Peña, J. Boon, S. Rojas, In Situ Conditioning of CO2-Rich Syngas during the Synthesis of Methanol, Catalysts 11 (2021) (2021) 534, https://doi.org/10.3390/CATAL11050534. Vol. 11, Page 534.
[40] T. Guo, Q. Guo, S. Li, Y. Hu, S. Yun, Y. Qian, Effect of surface basicity over the supported Cu-ZnO catalysts on hydrogenation of CO2 to methanol, J. Catal. 407 (2022) 312–321, https://doi.org/10.1016/J.JCAT.2022.01.035.
[41] S.K. Saw, S. Datta, P.D. Chavan, P.K. Gupta, S. Kumari, G. Sahu, V. Chauhan, Significance and influence of various promoters on Cu-based catalyst for synthesizing methanol from syngas: a critical review, J. Chem. Technol. Biotechnol. 98 (2023) 1083–1102, https://doi.org/10.1002/jctb.7331.
[42] J. Toyir, P. Ramírez De La Piscina, J. Luis, G. Fierro, N. Homs, Highly effective conversion of CO 2 to methanol over supported and promoted copper-based catalysts: influence of support and promoter, 2001.
[43] Q. He, Z. Li, D. Li, F. Ning, Q. Wang, W. Liu, W. Zhang, Y. Cui, J. Zhang, C. Liu, Mg enhanced the performance of Cu/ZnO/ZrO2 for CO2 hydrogenation to methanol and the mechanism investigation, Mol. Catal. 558 (2024) 114008, https://doi.org/10.1016/j.mcat.2024.114008.
[44] J. Schumann, M. Eichelbaum, T. Lunkenbein, N. Thomas, M.C. Álvarez Galván, R. Schlögl, M. Behrens, Promoting strong metal support interaction: Doping ZnO for enhanced activity of Cu/ZnO:M (M = Al, Ga, Mg) catalysts, ACS Catal. 5 (2015) 3260–3270, https://doi.org/10.1021/acscatal.5b00188.
[45] S.K. Sharma, T.S. Khan, R.K. Singha, B. Paul, M.K. Poddar, T. Sasaki, A. Bordoloi, C. Samanta, S. Gupta, R. Bal, Design of highly stable MgO promoted Cu/ZnO catalyst for clean methanol production through selective hydrogenation of CO2, Appl. Catal. A Gen. 623 (2021), https://doi.org/10.1016/j.apcata.2021.118239.
[46] H. Ren, C.H. Xu, H.Y. Zhao, Y.X. Wang, J. Liu, J.Y. Liu, Methanol synthesis from CO2 hydrogenation over Cu/γ-Al2O3 catalysts modified by ZnO, ZrO2 and MgO, J. Ind. Eng. Chem. 28 (2015) 261–267, https://doi.org/10.1016/j.jiec.2015.03.001.
[47] C. Zhong, X. Guo, D. Mao, S. Wang, G. Wu, G. Lu, Effects of alkaline-earth oxides on the performance of a CuO–ZrO 2 catalyst for methanol synthesis via CO 2 hydrogenation, RSC Adv. 5 (2015) 52958–52965, https://doi.org/10.1039/C5RA06508A.
[48] Z. Cheng, W. Zhou, G. Lan, X. Sun, X. Wang, C. Jiang, Y. Li, High-performance Cu/ZnO/Al2O3 catalysts for methanol steam reforming with enhanced Cu-ZnO synergy effect via magnesium assisted strategy, J. Energy Chem. 63 (2021) 550–557, https://doi.org/10.1016/j.jechem.2021.08.025.
[49] S.K. Sharma, T.S. Khan, R.K. Singha, B. Paul, M.K. Poddar, T. Sasaki, A. Bordoloi, C. Samanta, S. Gupta, R. Bal, Design of highly stable MgO promoted Cu/ZnO catalyst for clean methanol production through selective hydrogenation of CO2, Appl. Catal. A Gen. 623 (2021) 118239, https://doi.org/10.1016/J.APCATA.2021.118239.
[50] S. Ledakowicz, L. Nowicki, J. Petera, J. Nizioł, P. Kowalik, A. Gołębiowski, Kinetic characterisation of catalysts for methanol synthesis, Chem. Process Eng. 34 (2013) 497–506, https://doi.org/10.2478/cpe-2013-0040 (Inzynieria Chemiczna i Procesowa).
[51] F. Zhang, Y. Zhang, L. Yuan, K.A.M. Gasem, J. Chen, F. Chiang, Y. Wang, M. Fan, Synthesis of Cu/Zn/Al/Mg catalysts on methanol production by different precipitation methods, Mol. Catal. 441 (2017) 190–198, https://doi.org/10.1016/j.mcat.2017.08.015.
[52] J.M. Beiramar, A. Griboval-Constant, A.Y. Khodakov, Effects of metal promotion on the performance of CuZnAl catalysts for alcohol synthesis, ChemCatChem 6 (2014) 1788–1793, https://doi.org/10.1002/cctc.201402037.
[53] D. Previtali, M. Longhi, F. Galli, A. Di Michele, F. Manenti, M. Signoretto, F. Menegazzo, C. Pirola, Low pressure conversion of CO2 to methanol over Cu/Zn/Al catalysts. The effect of Mg, Ca and Sr as basic promoters, Fuel 274 (2020) 117804, https://doi.org/10.1016/j.fuel.2020.117804.
[54] S. Ay, M. Ozdemir, M. Melikoglu, Effects of metal promotion on the performance, catalytic activity, selectivity and deactivation rates of Cu/ZnO/Al2O3 catalysts for methanol synthesis, Chem. Eng. Res. Des. 175 (2021) 146–160, https://doi.org/10.1016/j.cherd.2021.08.039.
[55] P. Wang, H. Zhang, S. Wang, J. Li, Controlling H2 adsorption of Cu/ZnO/Al2O3/MgO with enhancing the performance of CO2 hydrogenation to methanol at low temperature, J. Alloy. Compd. 966 (2023) 171577, https://doi.org/10.1016/j.jallcom.2023.171577.
[56] Q. Chen, S. Meng, R. Liu, X. Zhai, X. Wang, L. Wang, H. Guo, Y. Yi, Plasma-catalytic CO2 hydrogenation to methanol over CuO-MgO/Beta catalyst with high selectivity, Appl. Catal. B 342 (2024), https://doi.org/10.1016/j.apcatb.2023.123422.
[57] F.M.T. Mendes L'a'b, M. Schmal A'c', APPLIED CATALYSIS The cyclohexanol dehydrogenation on Rh-Cu/A1203 catalysts" 2, Chemisorpt. React. (1997).
[58] S. Ren, X. Fan, Z. Shang, W.R. Shoemaker, L. Ma, T. Wu, S. Li, N.B. Klinghoffer, M. Yu, X. Liang, Enhanced catalytic performance of Zr modified CuO/ZnO/Al2O3 catalyst for methanol and DME synthesis via CO2 hydrogenation, J. CO2 Util. 36 (2020) 82–95, https://doi.org/10.1016/J.JCOU.2019.11.013.
[59] F. Song, W. Cheng, Y. Yu, Y. Cao, Q. Xu, Copper-doped ZnO-ZrO2 solid solution catalysts for promoting methanol synthesis from CO2 hydrogenation, R. Soc. Open Sci. 10 (2023) 221213, https://doi.org/10.1098/RSOS.221213.
[60] M. Behrens, D. Brennecke, F. Girgsdies, S. Kißner, A. Trunschke, N. Nasrudin, S. Zakaria, N.F. Idris, S.B.A. Hamid, B. Kniep, R. Fischer, W. Busser, M. Muhler, R. Schlögl, Understanding the complexity of a catalyst synthesis: Co-precipitation of mixed Cu,Zn,Al hydroxycarbonate precursors for Cu/ZnO/Al2O3 catalysts investigated by titration experiments, Appl. Catal. A Gen. 392 (2011) 93–102, https://doi.org/10.1016/J.APCATA.2010.10.031.
[61] W. Tong, A. West, K. Cheung, K.-M. Yu, S. Chi, E. Tsang, Dramatic Effects of Gallium Promotion on Methanol Steam Reforming Cu−ZnO Catalyst for Hydrogen Production: Formation of 5 Å Copper Clusters from Cu−ZnGaO x, 2013. https://doi.org/10.1021/cs400011m.
[62] W.J. Lee, A. Bordoloi, J. Patel, T. Bhatelia, The effect of metal additives in Cu/Zn/Al2O3 as a catalyst for low-pressure methanol synthesis in an oil-cooled annulus reactor, Catal. Today 343 (2020) 183–190, https://doi.org/10.1016/j.cattod.2019.03.041.
[63] S. Ay, M. Ozdemir, M. Melikoglu, Comparison of hydrogen consumption behavior of chromium and manganese promoted copper-based catalysts, Int J. Hydrog. Energy 46 (2021) 29173–29182, https://doi.org/10.1016/J.IJHYDENE.2020.11.204.
[64] T. Li, C. Fu, J. Qi, J. Pan, S. Chen, J. Lin, Effect of zinc incorporation manner on a Cu-ZnO/Al2O3 glycerol hydrogenation catalyst, React. Kinet. Mech. Catal. 109 (2013) 117–131, https://doi.org/10.1007/S11144-012-0538-X/TABLES/2.
[65] J.S. Lee, K.H. Lee, S.Y. Lee, Y.G. Kim, A comparative study of methanol synthesis from CO2/H2 and CO/H2 over a Cu/ZnO/Al2O3 catalyst, J. Catal. 144 (1993) 414–424, https://doi.org/10.1006/JCAT.1993.1342.
[66] X. Fang, Y. Men, F. Wu, Q. Zhao, R. Singh, P. Xiao, T. Du, P.A. Webley, Promoting CO2 hydrogenation to methanol by incorporating adsorbents into catalysts: Effects of hydrotalcite, Chem. Eng. J. 378 (2019) 122052, https://doi.org/10.1016/J.CEJ.2019.122052.
[67] P. Zhang, W. Wang, P. Wang, X. Mi, J. Xin, S. Li, Y. Wang, G. Liu, H. Wu, L. Tan, Tuning catalytic performance of CuZnOx catalyst via functional LaOx for catalyzing CO2 hydrogenation reaction, Mol. Catal. 573 (2025) 114818, https://doi.org/10.1016/J.MCAT.2025.114818.
[68] S. Chen, J. Zhang, F. Song, Q. Zhang, G. Yang, M. Zhang, X. Wang, H. Xie, Y. Tan, Induced high selectivity methanol formation during CO2 hydrogenation over a CuBr2-modified CuZnZr catalyst, J. Catal. 389 (2020) 47–59, https://doi.org/10.1016/J.JCAT.2020.05.023.